Pitot Pressure and Heat-Transfer Measurements in Hydrazine Thruster Plumes

H. Legge* and G. Dettleff†
Deutsche Forschungs- und Versuchsanstalt für Luft- und Raumfahrt, Göttingen, Germany

Pitot pressure and heat-transfer measurements have been made in plumes of 0.5-N (conical nozzle), 2-N, and 5-N (contoured nozzles) monopropellant hydrazine thrusters. The main objectives are to check the DFVLR simple plume model and to determine reliable model input values for real thrusters. The methods used for the heat-transfer measurements (applying a sphere probe), the recovery temperature determination, and the evaluation of the plume quantities relevant for plume impingement calculations are outlined. The Pitot pressure measurements showed the existence of shock disturbances in the near plume flowfield of the contoured nozzles. Stagnation temperatures between 900 and 1350 K were deduced from the measured recovery temperatures. The corresponding molecular weight range was found to be between 11 and 14.5 and the most reasonable mean effective ratio of specific heats to be $\kappa = 1.4 \pm 0.03$ for the expansion from the stagnation chamber to the continuum plume flow. This value is proposed for simple plume model calculations. The model heat-transfer results agree well with the experiments.

Nomenclature

A = area
c = constants
c_p, c_v = specific heat at constant pressure and volume, respectively
d = diameter
F = thrust
I_{sp} = specific impulse $I_{sp} = F/\dot{m}$
m = mass
M = molecular weight
Ma = Mach number
p = pressure
Pr = Prandtl number
$\dot{Q}$ = heat transfer
r = radius
r = recovery factor, Eq. (7)
R = specific gas constant
Re_2 = Reynolds number, Eq. (19)
St = Stanton number, Eq. (6)
t = time
T = temperature
u = velocity
x = centerline distance from nozzle exit
X_1 = dissociation degree of NH_3
δ'' = momentum thickness
θ_E = nozzle exit angle
κ = ratio of specific heats, $\kappa = c_p/c_v$
μ = viscosity
ρ = density

Subscripts

BL = boundary-layer (continuum) theory
cond = conduction
E = nozzle exit condition
FM = free molecule
K = in the vacuum chamber
lim = limiting condition for $Ma \to \infty$
loss = losses by radiation and conduction
off, on = thruster not firing and firing, respectively
r = at recovery condition
rad = radiation
s = sphere
u = velocity
w = at the wall, sphere probe condition
0 = stagnation condition
1 = freestream
2 = condition behind a normal shock wave

Superscripts

1,2,... = number of iteration
$(\ )^*$ = nozzle throat
$(\dot{\ })$ = time derivative

Introduction

IN a previous study, existing analytical plume flow models[1-3] were extended to deliver all flow quantities relevant to impingement calculations. Free-molecular plume flow was included by the definition of a freezing surface.[4,5] In this DFVLR model, constant composition flow is assumed with mean constant gas properties. The angular plume flow description is most sensitive to changes in the ratio of specific heats of the exhaust gases.

The present work is part of an extensive study of plume flow and impingement effects on spacecraft surfaces, that serves to test, verify, and improve the model by analyzing systematically the influence of the thruster nozzle geometry, nozzle boundary layer, and ratio of specific heats using pure gases.[6]

This paper deals with experiments in real hydrazine plume flows from three different thrusters of the German aerospace company MBB/ERNO.

Experiment

The setup in the MBB/ERNO high-vacuum test facility is sketched in Fig. 1. The DFVLR Pitot and heat-transfer probes were positioned in the plume by a three-axis remotely controlled traversing mechanism. The thrust F, the mass flow $\dot{m}$, and the stagnation pressure p_0 were measured by MBB/ERNO during both pulse mode and steady-state firings. The background pressure in the vacuum tank was between 3 and 40 N/m^2 when the thrusters were firing. The on- and off-times of the fuel valve during the pulse mode tests were $t_{on} = 0.1$ s, $t_{off} = 0.9$ s and $t_{on} = 0.3$ s, $t_{off} = 2.7$ s for the 0.5-N thruster and $t_{on} = 0.25$ s, $t_{off} = 0.75$ s for the 2-N and 5-N thrusters. The thruster assembly consists of a flow control valve, a decomposition chamber with catalyst bed, thermal control heaters, and the nozzle. The geometries of the three different nozzles are depicted in Fig. 2.

Presented as Paper 85-0934 at the AIAA 20th Thermophysics Conference, Williamsburg, VA, June 19-21, 1985; revision received Jan. 4, 1986.

*Scientist, Institute for Experimental Fluid Mechanics. Member AIAA.
†Scientist, Institute for Experimental Fluid Mechanics.

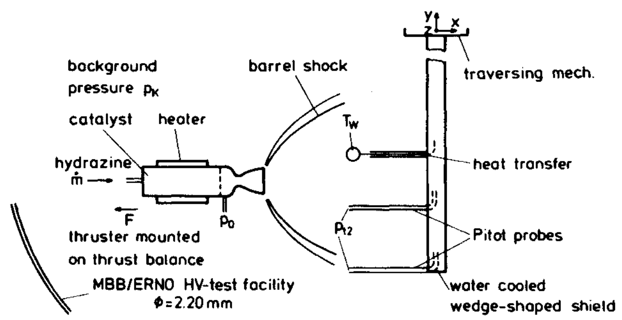

Fig. 1 Experimental setup.

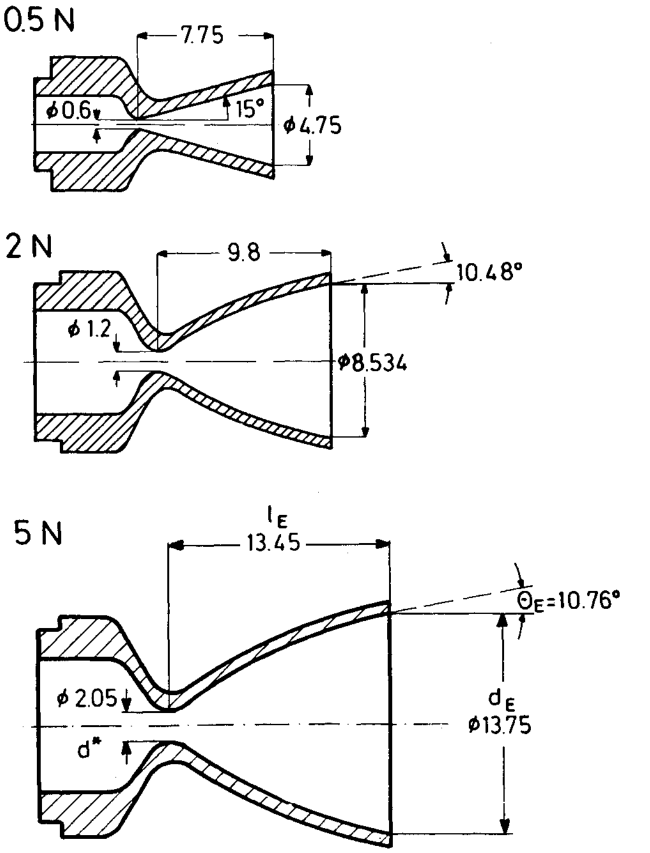

Fig. 2 Nozzle geometries of thrusters with a nominal thrust of 0.5, 2, and 5 N, in mm.

Two Pitot pressure probes with diameters of 2 and 6 mm were used. The larger one was employed to avoid corrections due to rarefaction. The heat-transfer probe is depicted in Fig. 3. A copper sphere coated with electroplated nickel of 2-μ thickness was supported by a stainless steel tube enclosing a thermocouple by which the temperature of the sphere was measured. A second tube shields and supported the smaller one.

The temperature was recorded as a function of time from the start of the thruster firing until the probe reached a temperature $T_w \approx 800$ K. The probe was used as calorimeter, having a response time of approximately 10 ms. An example of the temperature recording of a number of pulses, together with the thruster performance data, is given in Fig. 4, where F is the thrust, $m = \int \dot{m} dt$ (over one pulse), $\dot{m}$ is the mass flow, p_0 is the stagnation pressure, and $I_{sp} = \int F dt/m$ (over one pulse) is the specific impulse.

The total heat transfer to the sphere consists of the aerodynamic part $\dot{Q}$ and the heat losses $\dot{Q}_{loss}$ by radiation and conduction:

$$\dot{Q}_{tot} = \dot{Q} + \dot{Q}_{loss} = m_s c_s (dT_w/dt) \tag{1}$$

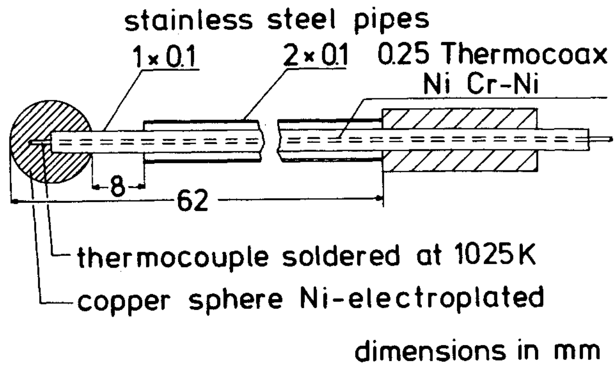

Fig. 3 Heat-transfer probe.

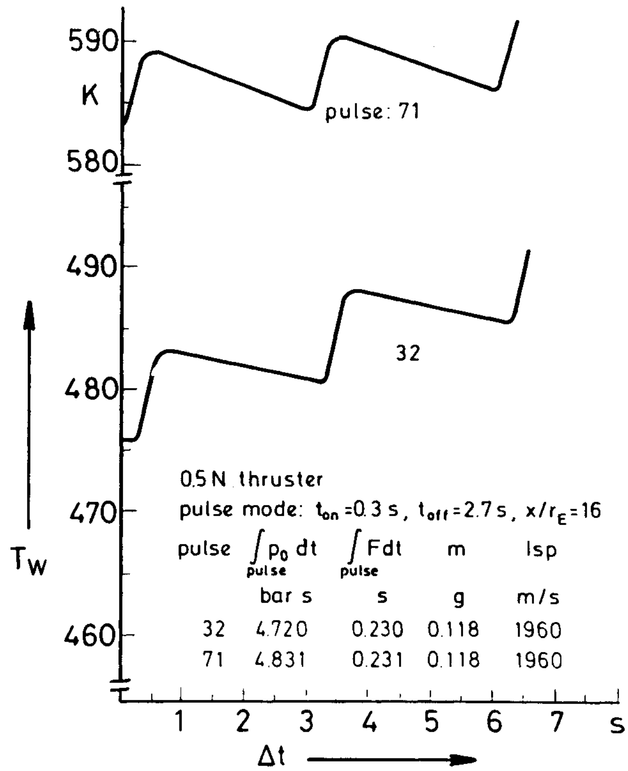

Fig. 4 Example of probe temperature recording and thruster performance data for pulse mode firing of a 0.5-N thruster.

where m_s and c_s are the mass and specific heat of the sphere, respectively. The losses at a certain T_w were determined by the temperature decrease during the off-time in the pulse mode firing of the thruster

$$\dot{Q}_{loss} = m_s c_s (dT_w/dt)_{loss} = m_s c_s (dT_w/dt)_{off} \tag{2}$$

The losses could be approximated by the equation

$$-\frac{\dot{Q}_{loss}}{m_s c_s} = -\left(\frac{dT_w}{dt}\right)_{loss} = c_{rad}(T_w^4 - T_a^4) + c_{cond}(T_w - T_a) \tag{3}$$

where $Ta \approx 300$ K is the ambient temperature and the constants are $c_{rad} = 7.3 \times 10^{-12}$ $(1/K^3 s)$ and $c_{cond} = 3 \times 10^{-4} (1/s)$.

For steady-state tests dT_w/dt was determined directly from the slope of the temperature-time curves. For the pulse mode tests, the temperature steps for one or n ($n = 6$) pulses were used as shown in Fig. 5. This figure gives an example of the temperature recording during a pulse mode test with $\Delta t_{on} := t_{on} = 0.1$ s, $\Delta t_{off} := t_{off} = 0.9$ s.

The total heat transferred to the sphere during the time of n pulses is

$$\Delta Q_{\mathrm{tot},n} = m_s \cdot c_s \cdot \Delta T_{w,n} = \int_{t_0}^{t_n} (\dot{Q} + \dot{Q}_{\mathrm{loss}}) \mathrm{d}t$$
$$\approx n\dot{Q}\Delta t_{\mathrm{on}} + n\dot{Q}_{\mathrm{loss}} (\Delta t_{\mathrm{on}} + \Delta t_{\mathrm{off}}) \tag{4}$$

Solving Eq. (4) for the average aerodynamic heat transfer $\dot{Q}$ at the mean temperature $T_{w,n}$, we obain

$$\dot{Q} = m_s c_s \left[\frac{\Delta T_{w,n}}{n\Delta t_{\mathrm{on}}} - \left(\frac{\mathrm{d}T_w}{\mathrm{d}t} \right)_{\mathrm{loss}} \cdot \frac{\Delta t_{\mathrm{on}} + \Delta t_{\mathrm{off}}}{\Delta t_{\mathrm{on}}} \right] \tag{5}$$

Heat-Transfer Model

To describe the heat transfer of blunt bodies (here the sphere probe) not only in continuum and free-molecular flow but also in transition flow, a bridging method for the transition regime has been used for the Stanton number and recovery factor, which are defined by

$$St = \frac{\dot{Q}}{\rho_1 u_1 c_p (T_r - T_w) A_s} \tag{6}$$

$$r = \frac{T_r - T_1}{T_0 - T_1} \tag{7}$$

where T_r is the recovery temperature, ρ_1, u_1, and T_1 are the freestream density, velocity, and temperature, respectively, and c_p is the mean specific heat at constant pressure for the exhaust gas mixture. A_s is the projected area of the blunt body. For the bridging we have

$$St = St_{\mathrm{FM}} \cdot \frac{2.6}{\sqrt{Re_2 + 6.7}} \tag{8}$$

$$r = r_{\mathrm{FM}} - \frac{r_{\mathrm{FM}} - r_{\mathrm{BL}}}{\lg 100 - \lg 2} (\lg Re_2 - \lg 2), \quad 2 \le Re_2 \le 100 \tag{9}$$

$$r = r_{\mathrm{FM}} \text{ for } Re_2 < 2 \tag{10}$$

$$r = r_{\mathrm{BL}} = \sqrt{Pr} \approx \sqrt{4/\left(9 - \frac{5}{\kappa}\right)}, \quad Re_2 > 100 \tag{11}$$

where Pr is the Prandtl number, κ the ratio of specific heats, and Re_2 the Reynolds number behind a normal shock wave based on the sphere diameter d_s. The indices FM and BL indicate free-molecular and laminar boundary-layer flow. The free-molecular values have been calculated for complete accommodation. The formulas were derived from measurements of spheres and cones with half-angles between 15 and 90 deg (flat plate). The recovery factor was specified for the sphere by the experimental value 0.92 for air[8] and varied with κ according to

$$r_{\mathrm{BL},s} = 0.92 \cdot \frac{\sqrt{Pr(\kappa)}}{\sqrt{Pr(\kappa = 1.4)}} \tag{12}$$

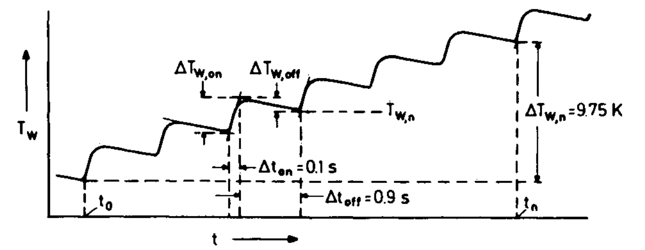

Fig. 5 Quantities for data reduction using n pulses of the temperature recording. Example for 0.5-N thruster with $t_{\mathrm{on}} = 0.1$ s, $t_{\mathrm{off}} = 0.9$ s.

Experimental Results

Pitot Pressure Measurements

The Pitot pressure $p_{t2}(x)$ along the centerline and perpendicular to it $p_{t2}(y)$ has been recorded during steady-state firings. Examples of $p_{t2}(y)$ are given for the 0.5-N thruster in Fig. 6 and for the 5-N thruster in Fig. 7. The 0.5-N thruster that showed smooth Pitot pressure profiles has a conical nozzle with a half-angle $\theta_E = 15$ deg (see Fig. 2). The other two contoured nozzles exhibited shocks and compression zones by steep p_{t2} rises (see Fig. 7). The shock can originate from a recompression of an overexpansion at the nozzle throat or from the contour of the supersonic nozzle region.

Figure 8 shows an axisymmetric shock system in a conical nozzle and how it influences a streamline. The last shock wave at the nozzle wall turns the flow onto the centerline. The Mach number behind this shock is decreased. Together with the effect of the last shock in the plume, this supports the spreading of the flow.

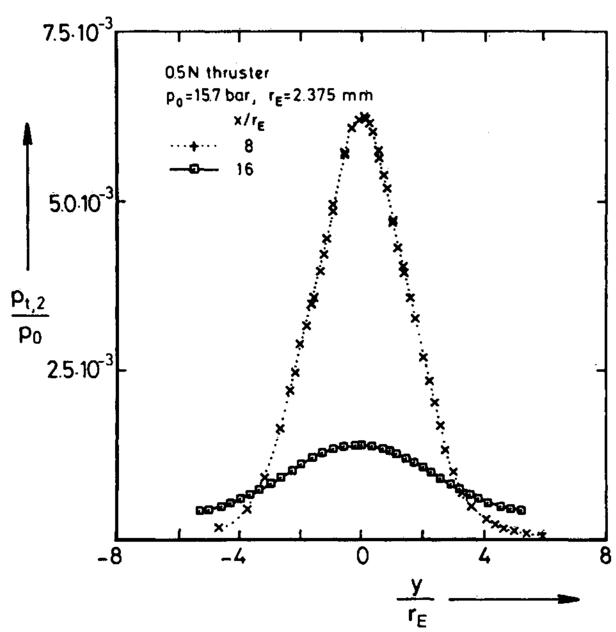

Fig. 6 Pitot pressure $p_{t2}(y)$ for 0.5-N thruster.

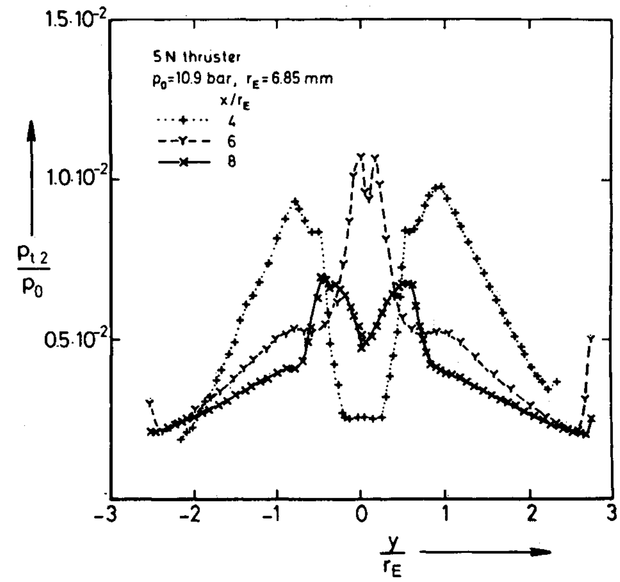

Fig. 7 Pitot pressure $p_{t2}(y)$ for 5-N thruster.

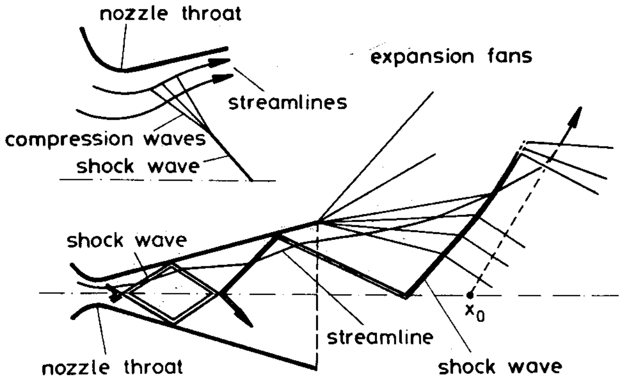

Fig. 8 Scheme of a possible shock pattern and streamlines in a nozzle and a plume expanding into vacuum.

Another shock pattern can be found in a short contoured nozzle with a large expansion near the nozzle throat. In this nozzle, the shock and flow pattern is expected to be similar to that of a freejet expanding into still air if the nozzle contour follows approximately the boundary of such a jet. The peaks of the profiles $p_{t2}(y)$ indicate this type of shock pattern for the 2-N and 5-N thrusters as suggested by the dashed line in Fig. 9, which extrapolates the Pitot pressure peaks into the nozzle.

The influence of these shocks on the entropy s and on the total pressure loss at the plume centerline can be estimated by the relation for oblique shocks

$$e^{-\Delta s/R} = \frac{p_{01}}{p_{02}} = f(\kappa, Ma_1, \beta) \tag{13}$$

where R is the specific gas constant, p_{01}/p_{02} the total pressure ratio across an oblique shock, Ma_1 the freestream Mach number in front of the shock, and β the shock angle. For the 2-N and 5-N thrusters, we found an angle between the center streamline and the shock in the plume of $\beta \approx 10$ deg (see Fig. 9). Assuming that $\kappa = 1.4$, we estimate from p_{t2}/p_0 the Mach number Ma_1 and obtain from the 2-N and 5-N thrusters $p_{01}/p_{02} < 1.1$.

The overall effect of the shocks on the plume flow is dependent on the strength and location of the shocks and on their interference with the nozzle boundary layer. In some cases, these shocks will have a large influence on the density in the plume. In these cases, theoretical approximations without any measurements seem questionable. Further results of the Pitot pressure measurements are given in Ref. 7.

Heat-Transfer Measurements

The aerodynamic heat transfer is shown in Fig. 10 per unit frontal area $A_s = \pi r_s^2$ as a function of T_w for steady-state mode firing of a 0.5-N thruster. In the table in Fig. 10, the axial probe distance x/r_E in nozzle exit radii, p_0, and the best-fit straight line through the experimental points

$$\dot{Q}/A_s = c_1 \cdot T_w + c_2 \tag{14}$$

are given. [It is assumed that the Stanton number is not dependent on T_w; see Eq. (6)]. When the thruster starts to fire and has not reached its best performance, $\dot{Q}/A_s$ is not representative for the entire test. Therefore, these first points, indicated in the column headed "I>", are omitted in the calculation of the best fit. The extrapolation of $\dot{Q}/A_s = f(T_w)$ by the best-fit straight line to $\dot{Q}/A_s = 0$ determines the recovery temperature

$$T_r = -c_2/c_1 \tag{15}$$

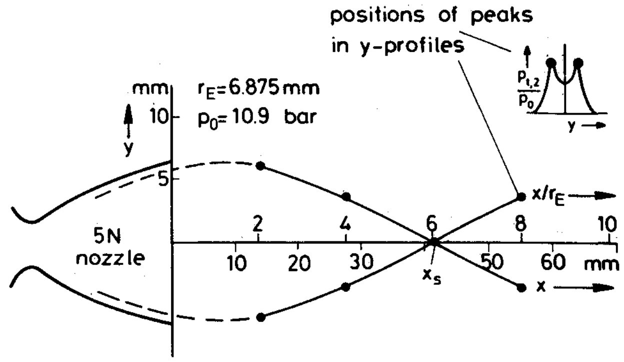

Fig. 9 Main shock structure in the plume of 5-N thruster.

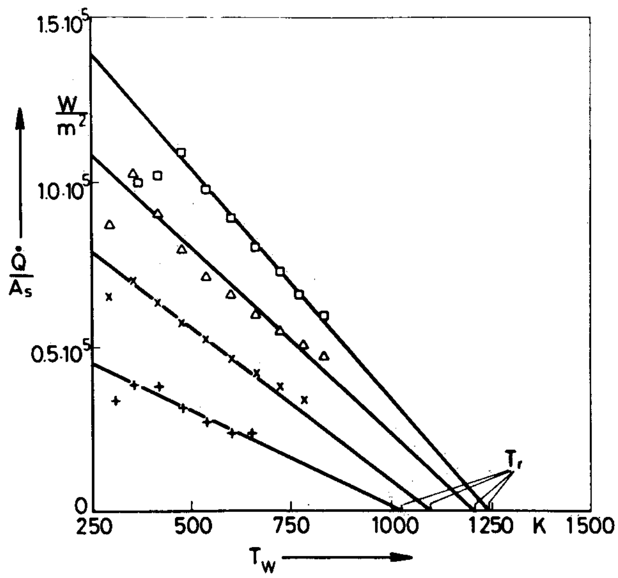

0.5 N thruster, steady state

	x/r_E	p_0 [bar]	$(p_{t,2}/p_0)\cdot 10^3$	$\dot{Q}/A_s$ [W/m²]	I>
□	32	15.6	0.270	$-139.70 \cdot T_w + 174\,600$	2
△	40	15.8	0.171	$-112.80 \cdot T_w + 137\,100$	1
×	32	7.95	0.239	$-84.69 \cdot T_w + 99\,120$	1
+	32	4.56	0.213	$-58.74 \cdot T_w + 60\,650$	1

Fig. 10 Aerodynamic heat transfer on the sphere probe and recovery temperature determination for different stagnation conditions and probe distances.

Combination of Pitot Pressure, Heat Transfer, Stagnation Pressure, Mass Flow, and Thrust

The measured quantities p_{t2}, $\dot{Q}$, T_r, p_0, $\dot{m}$, and F were combined to deliver freestream plume flow quantities in a number of different ways. All relevant plume flow quantities, including T_0, a mean molecular weight M, and an effective κ value for the nozzle and plume flow, were determined in an iteration procedure that can be roughly characterized by

$$\kappa^1, M^1, F, \dot{m}, p_0, p_{t2}, T_r \rightarrow Re_2^1, r^1, T_0^1 \rightarrow \kappa^2, M^2$$
$$\rightarrow \kappa^2, M^2, F, \dot{m}, p_0, p_{t2}, T_r \rightarrow Re_2^2 \ldots$$

A three-step iteration was sufficient for stable results.

The velocity and density in the plume were determined from a correction of the specific impulse $I_{sp} = F/\dot{m}$ and from the Pitot pressure p_{t2}. In this calculation, κ has only a minor influence on the result. The nozzle exit velocity is determined from

$$u_E = \frac{F}{\dot{m}} \left(1 - \frac{(p_E - p_K) A_E}{F}\right) \Big/ \left[\frac{1 + \cos\theta_E}{2} \left(\frac{r_E - \delta_E''}{r_E}\right)^2\right] \tag{16}$$

where p_K is the surrounding (chamber) pressure and where p_E, A_E, θ_E, r_E, δ_E'' are the pressure, area, contour angle, radius, and momentum thickness, respectively, at the nozzle exit. The freesteam velocity u_1 is obtained by the correction of u_E

$$\frac{u_1}{u_E} \approx \sqrt{1+\frac{2}{\kappa-1}\left(\frac{1}{Ma_E^2}-\frac{1}{Ma_1^2}\right)} \tag{17}$$

Knowing u_1 the density is determined from the Pitot pressure by the hypersonic approximation

$$\rho_1 \approx p_{t2}\cdot\frac{\kappa+3}{2(\kappa+1)}\Big/u_1^2 \tag{18}$$

In this formula, the assumed κ (at the location of the Pitot probe) has only a small influence on the resulting ρ_1. To calculate u_E and u_1 by Eqs. (16) and (17), standard formulas are used for the determination of p_E, δ_E'', and $Ma_1(p_{t2}/p_0)$.

T_0, M, and κ are derived in the iteration as follows. T_0 results from the experimental T_r and the recovery factor given by Eqs. (7) and (9-12). The recovery factor, and thereby the determination of T_0, is only weakly dependent on κ and T_1. Therefore, we can use $\kappa=1.4$, $\mu(T_2)=\mu(T_r)$, together with Eqs. (16-18), for a first estimation of Re_2 and T_0 with

$$Re_2=\frac{\rho_2\cdot u_2\cdot d_s}{\mu(T_2)}=\frac{\rho_1\cdot u_1\cdot d_s}{\mu(T_2)} \tag{19}$$

Assuming[9]

$$3N_2H_4 \rightarrow 4(1-X_1)NH_3+(1+2X_1)N_2+6X_1H_2$$
$$+(3.35-1.84X_1)\cdot 10^5\,J \tag{20}$$

to be the overall decomposition of N_2H_4, the dissociation degree X_1 of NH_3 and M can be calculated by

$$X_1=[1649-T_0(K)]/782 \tag{21}$$

$$M=96.14/(5+4X_1) \tag{22}$$

We assume constant composition flow; and, for $X_1>0.3$, use the approximation for the ratio of specific heats in the stagnation chamber of

$$\kappa_0=1.14+0.23X_1 \qquad (X_1>0.3) \tag{23}$$

The differently derived plume flow quantities, especially the limiting velocity $u_{\lim}=u(Ma\rightarrow\infty)$ determined by the energy equation from T_0

$$\frac{u_{\lim}^2}{2}=\frac{\kappa}{\kappa-1}\cdot R\cdot T_0 \tag{24}$$

and by Eqs. (16) and (17) from the specific impulse $I_{sp}=F/\dot{m}$, agreed best for an effective $\kappa=1.4\pm0.03$. This κ range is covered in the iteration by the assumption

$$\kappa=(\kappa_0+1.5)/2 \tag{25}$$

An accurate determination[7] of an effective κ particularly suitable in describing the plume spreading resulted in $\kappa=1.37$ in agreement with the present result. Therefore, it seems sufficient to use one effective κ in the model to calculate near-axis plume flow quantities of monopropellant hydrazine thrusters.

The experimental T_r and the deduced T_0 are given in Fig. 11. T_0 varied between 900 and 1350 K. The largest values were obtained for the largest p_0 with the 0.5-N thruster. Corresponding to T_0, the range of molecular weight is $11<M<14.5$.

The differently derived limiting velocities, $u_{\lim}$ (I_{sp}) using Eqs. (16) and (17) for $Ma_1\rightarrow\infty$ and $u_{\lim}$ (T_0,κ,M) using Eq.

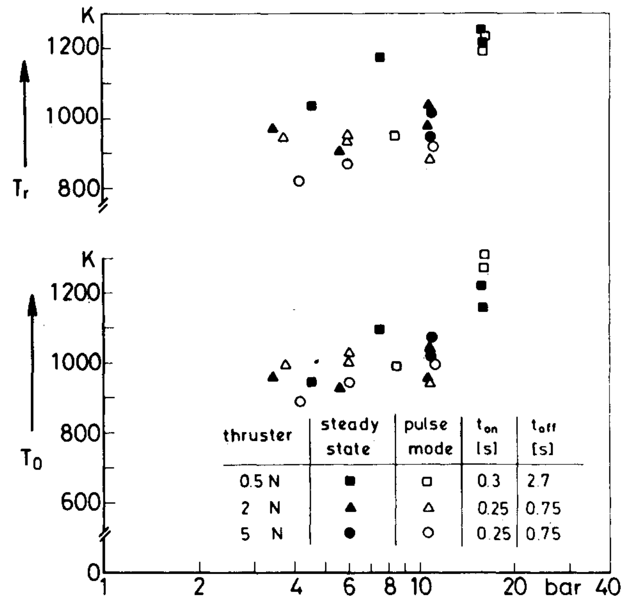

Fig. 11 Recovery and stagnation temperatures for different thrusters, firing modes, and stagnation conditions.

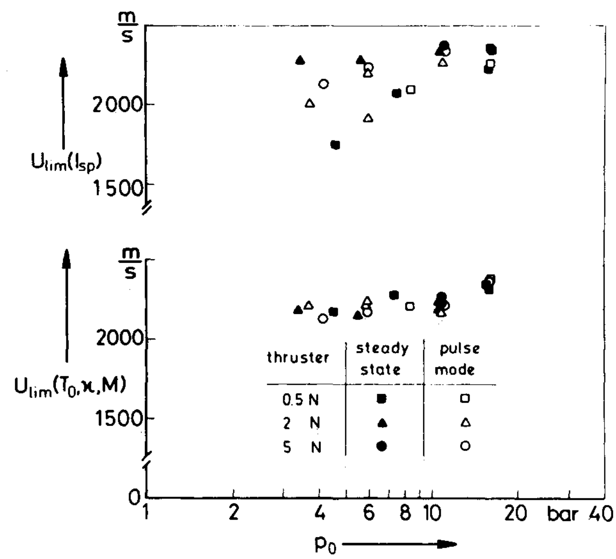

Fig. 12 Limiting velocities ($Ma_1\rightarrow\infty$) derived from the specific impulse and the stagnation temperature for different thrusters, firing modes, and stagnation conditions.

(24), are given in Fig. 12 and agree well [except for the scattering in $u_{\lim}$ (I_{sp})] justifying the assumptions.

Comparison of Experimental and Model Calculations

The model calculations[5-7] of $\dot{Q}/A_s$ and p_{t2}/p_0 are directly compared to the experimental results of the steady-state firings in Figs. 13 and 14, respectively. The model calculations are done for constant composition flow, with $M=14.5$, $T_0=1345$ K, $\kappa=1.24$, and $\kappa=1.4$. The value $\kappa=1.24$ corresponds to T_0 [Eqs. (21) and (23)] and was used in the past. The calculated heat transfer is not strongly dependent on κ and is in good agreement with the experimental results. The model Pitot pressure values agree much better with the experimental results when a κ of 1.4 is assumed; however, the model results are still smaller than the experimental values. This is essentially due to a different source point in the experiments than assumed up to now (near the nozzle exit) in the model and also to a different nozzle boundary-layer influence.[7]

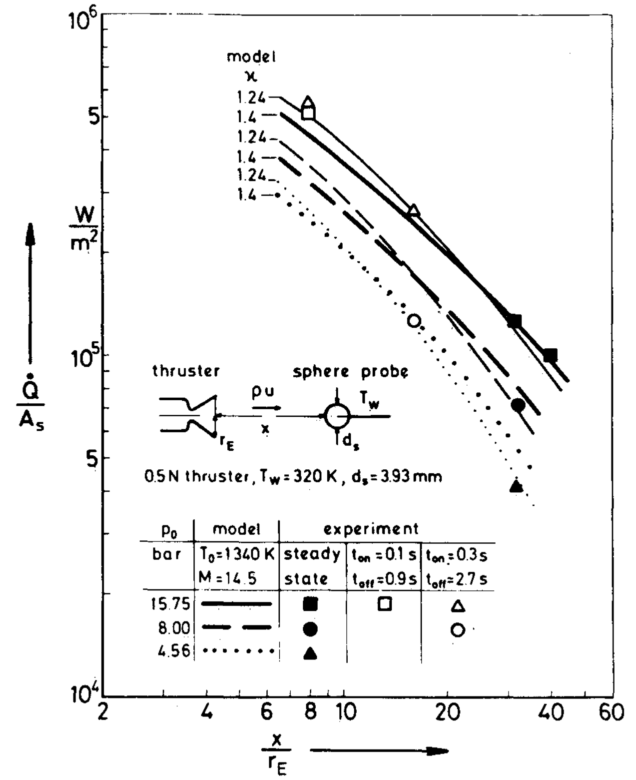

Fig. 13 Comparison between model and experimental heat-transfer results.

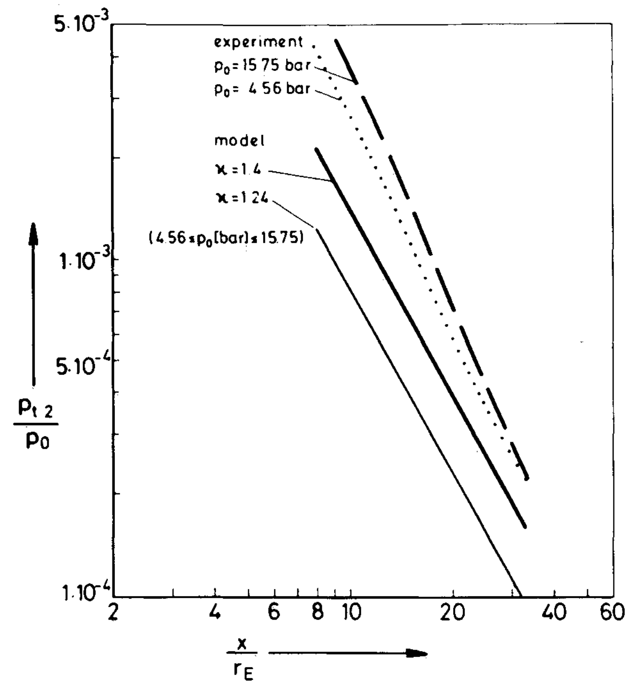

Fig. 14 Comparison between model and experimental Pitot pressure results.

Conclusions

Pitot pressure measurements in plumes of monopropellant hydrazine thrusters showed the existence of compression waves and shocks indicated by steep rises in Pitot pressure profiles. These shocks are due to the interaction between the nozzle contour and the expanding gas and influence the centerline and angular pressure profiles (especially since the nozzle boundary-layer expansion region of the plume will probably be changed. This region is most important for most impingement problems). Simple analytical model calculations seem especially justified for nozzles without shocks.

Heat-transfer and recovery temperature measurements resulted in stagnation temperatures that ranged from 900 to 1350 K. The corresponding molecular weight range is $11 < M < 14.5$. A mean effective ratio of specific heats, $\kappa = 1.4 \pm 0.03$ (for the nozzle and plume expansion process), agreed best with the experimental measurements reported here and also with the value resulting from plume spreading measurements.[7]

On the centerline of the plume, the model heat-transfer description is not very sensitive to changes in κ and agrees well with the experiments. As shown especially by the Pitot pressure measurements, the ratio of specific heats in the plume model[5] should be changed from $\kappa = 1.24$ (used up to now) to $\kappa = 1.4$ when plume impingement occurs near the centerline.

Acknowledgment

This work was supported by the European Space Agency through Contract ESTEC 5194-82-NL-PB (SC).

References

[1]Boynton, F.P., "Highly Underexpanded Jet Structure. Exact and Approximate Calculations," *AIAA Journal,* Vol. 5, Sept. 1967, pp. 1703-1705.

[2]Simons, G.A., "Effect of Nozzle Boundary Layers on Rocket Exhaust Plumes," *AIAA Journal,* Vol. 10, Nov. 1972, pp. 1534-1535.

[3]Lengrand, J.C., Allegre, J., and Raffin, M., "Experimental Investigation of Underexpanded Exhaust Plumes," *AIAA Journal,* Vol. 14, May 1976, pp. 692-694.

[4]Legge, H. and Boettcher, R.D., "Modelling Control Thruster Plume Flow and Impingement," *Proceedings of the 13th International Symposium on Rarefied Gas Dynamics,* Plenum Press, New York, 1985, pp. 983-992.

[5]Boettcher, R.D., Dettleff, G., Koppenwallner, G., and Legge, H., "A Study of Rocket Exhaust Plumes and Impingement Effects on Spacecraft Surfaces," European Space Agency Rept. ESA CR (P)-1698, 1982.

[6]Legge, H., Dankert, C., and Dettleff, G., "Experimental Analysis of Plume Flow from Small Thrusters," *Proceedings of the 14th International Symposium on Rarefied Gas Dynamics,* Vol. 1, University of Tokyo Press, Tokyo, Japan, 1984, pp. 279-286.

[7]Dettleff, G., Boettcher, R.D., Dankert, D., Koppenwallner, G., and Legge, H., "Attitude Control Thruster Plume Flow Modelling and Experiments," AIAA-Paper 85-9833, 1985.

[8]Eberly, D.K., "Forced Convection Heat Transfer from Spheres to a Rarefied Gas," Engineering Research Dept., University of California, Berkeley, HE-150-140, 1956; see also Springer, G.S., "Heat Transfer in Rarefied Gases," *Advances in Heat Transfer,* Vol. 7, edited by T.F. Irvine and J.P. Hartnett, Academic Press, New York, London, 1971, pp. 163-218.

[9]Altman, D. and Penners, S.S., "Combustion of Liquid Propellants, High Speed Aerodynamics and Jet Propulsion," *High Speed Aerodynamics and Jet Propulsion,* Vol. II, New York, London, edited by B. Lewis, R.N. Pease, and H.S. Taylor, Princeton University Press, Princeton, NJ, 1956, Sec. L.